

TA7
Cb
CER-70-71-7
Ap. 2

Technical Report

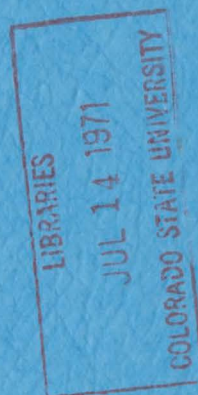
A STUDY ON THREE DIMENSIONAL
CHANGE IN ROUGHNESS

by

K. D. Nambudripad

and

J. E. Cermak



Technical Report

A STUDY ON THREE DIMENSIONAL
CHANGE IN ROUGHNESS

by

K. D. Nambudripad

and

J. E. Cermak

August 1970

CER70-71KDN-JEC7

LIST OF FIGURES

<u>Figure</u>		<u>Page</u>
1	Wind tunnel	
2	Experimental arrangement.	
3	Schematic diagram of the electric bridge for the force dynamometer strain-gauges	
4	Calibration curve for shear plate	
5	Calibration curve for force dynamometer	
6	Variation of local drag coefficient with Reynolds number for smooth and rough surfaces.	
7	Variation of local drag coefficient with momentum thickness Reynolds number.	
8	Variation of c_f after roughness change force dynamometer measurements.	
9	Typical log-law velocity profiles over smooth and rough surfaces	
10a	Variation of mean velocity profiles over rough surface.	
b	Velocity profiles downstream of roughness	
11	Velocity profiles over the rough surface at Station 4	
12a through i	Power law velocity profiles over the smooth and rough surfaces.	
13	Variation of U/U_∞ with $y^{1/2}$	
14	Variation of $\frac{u_*^k}{v}$ with R_{xe} at Station 1 through 7	

LIST OF SYMBOLS

<u>Symbol</u>	<u>Definition</u>
A	Constant
B	Constant
C_f	Local drag coefficient = $\tau_o / \frac{1}{2} \rho U_\infty^2$
H	Shape factor = δ_*/θ
k	Height of roughness (L)
n	Constant
R_x	Reynolds number = $\frac{U_\infty x}{\nu}$
R_{x_e}	Effective Reynolds number = $\frac{U_\infty x_e}{\nu}$
R_θ	Momentum thickness Reynolds number = $\frac{U_\infty \theta}{\nu}$
U	Local mean velocity in x-direction (L/T)
U_∞	Free stream velocity
u_*	Shear velocity = $\sqrt{\tau_o / \rho}$
x	Longitudinal distance along wind tunnel (L)
x_e	Effective distance calculated from eq. (4) (L)
k	Distance downstream from the roughness discontinuity (L)
y	Distance normal to surface measured from wall (L)
δ	Boundary layer thickness (L)
δ_*	Displacement thickness = $\int_0^\infty (1 - \frac{U}{U_\infty}) dy$ (L)
θ	Momentum thickness = $\int_0^\infty \frac{U}{U_\infty} (1 - \frac{U}{U_\infty}) dy$ (L)
ν	Kinematic viscosity of fluid (L^2/T)
ρ	Mass density of fluid (M/L^3)
τ_o	Wall shear stress (M/LT^2)

CHAPTER 1

INTRODUCTION

This study is part of a program on laboratory simulation of urban diffusion. One of the problems that arises in the modeling of a city in a laboratory wind tunnel is the similarity of the surface characteristics in the field and in the model. Changes in surface features such as buildings considerably affect the flow over them, that the problem warrants a detailed investigation for understanding the effects of such changes. This forms the basis of the laboratory investigation undertaken, the results of which are reported here. The investigation is presently restricted to direct measurements of the surface shear stress and mean velocity profiles when a finite size of uniform roughness is placed on the otherwise smooth wind tunnel floor. At the present stage only one size and pattern of roughness has been studied.

While modeling very large areas, say over five miles width and more, in a wind tunnel the length scales become very large, making the vertical dimensions so small that the model surface may act as aerodynamically smooth surface. The effective roughness of the different parts of the area may not, therefore, be truly simulated in the model. This necessitates the choice of an exaggerated vertical scale in order to provide an aerodynamically rough surface. It

is, therefore, necessary to know the extent of this vertical distortion for proper similarity to exist between the prototype and the model.

A surface may be considered aerodynamically "fully rough" if the average height of the roughness protuberances is significantly larger than the thickness of the viscous sublayer, so that the viscous effects on the flow are completely destroyed. In other words, a fully rough surface is considered to exist when the parameter $\frac{u_* k}{\nu}$ is larger than about 70, though smaller values of even 55 (Hinze [71]) have been recommended. Here u_* is the shear velocity $= \sqrt{\tau_o / \rho}$, k is the average height of the roughness and ν is the kinematic viscosity of the fluid. On the other hand we may also consider a surface to be fully rough when the local drag coefficient is no longer dependent on the Reynolds number of the flow. For the 0.25 in. roughness used in this study these characteristics were tested for the usual Reynolds numbers encountered in the wind tunnel flows. The measured drag coefficients refer mainly to the average values for the entire area of the rough surface and only some exploratory study for the local drag coefficients are reported here.

CHAPTER 2

BACKGROUND

Skin-friction Formulae for Smooth and Rough Surfaces: --

The momentum integral equation for a turbulent boundary layer developing along a flat plate at zero pressure gradient has been shown (see Schlichting [19]) to take a simple form:

$$\tau_o = \rho U_\infty^2 \frac{d\theta}{dx} \quad (1)$$

or in terms of the local drag coefficient,

$$c_f = \tau_o / \frac{1}{2} \rho U_\infty^2 = 2 \frac{d\theta}{dx} \quad (2)$$

Using this relation and Nikuradse's smooth pipe flow data and assuming 1/7th power law velocity distribution in the boundary layer Schlichting obtained the relation

$$c_f = 0.0592 \left(\frac{U_\infty x}{\nu} \right)^{-1/5} \quad (3)$$

Using the derived relation

$$\theta(x) = 0.036x \left(\frac{U_\infty x}{\nu} \right)^{-1/5} \quad (4)$$

he gets another formula

$$c_f = 0.0256 \left(\frac{U_\infty x}{\nu} \right)^{-1/4} \quad (5)$$

Any change in the power law exponent alters only the numerical constant.

When a logarithmic velocity distribution was used, Schlichting obtained an empirical best fit relation

$$c_f = (2 \log R_x - 0.65)^{-2.3} \quad (6)$$

Where $R_x = \text{Reynolds number} \frac{U_\infty x}{\nu}$.

Schultz Grunow [21] used the universal velocity defect law to obtain an interpolation formula

$$c_f = 0.37 (\log R_x)^{-2.584} \quad (7)$$

Nikuradse [19] using the similarity relation $u/u_\infty = f(y/\delta_*)$, where y is the height above the surface and δ_* the displacement thickness, obtained

$$c_f = 0.023 R_x^{-0.139} \quad (8)$$

and found that the shape parameter, $H = \delta_*/\theta = \text{const} = 1.30$.

Hama [6] has shown that most of the existing drag coefficient formulations can be reduced to the form:

$$\frac{U_\infty}{u_*} = \sqrt{\frac{2}{c_f}} = A \log \frac{U_\infty \theta}{\nu} + B \quad (9)$$

where the numerical constants A and B have average values of about 5.75 and 4.5 respectively.

Rotta [18] showed that if a mean velocity profile composed of the universal law of the wall and a one parameter velocity defect law is adopted, the local drag coefficient will then have the general functional form

$$c_f = c_f \left(\frac{U_\infty \theta}{\nu}, H, k/\theta \right) \quad (10)$$

which reduces, for a smooth surface, to

$$c_f = c_f \left(\frac{U_\infty \theta}{\nu}, H \right) \quad (11)$$

The experimental results of Schubauer and Klebanoff [20] and Ludwig and Tillman [13] shows that c_f decreases when the shape parameter H increases. The latter authors derived the approximate formula

$$c_f = 0.246 \times 10^{-0.678H} \left(\frac{U_\infty \theta}{\nu} \right)^{-0.268} \quad (12)$$

which yields, for $\frac{U_\infty \theta}{\nu} > 1000$ and $H < 2$ essentially the same results as Rotta's formulation.

For boundary layer flows over a uniformly rough plate a convenient method for finding out its behaviour is to use an equivalent sand grain roughness, k_s . This has been defined as that value of the standard (Nikuradse) sand-grain roughness height which gives the same resistance as the given roughness. Using Nikuradse's formulations for the velocity distribution over the standard sand-roughened surface it is possible to correlate any homogeneous rough surface with the standard one. However the validity of this correlation is questionable when the roughness is not homogeneous over the surface such as in the present case of a finite size of rough area on an otherwise smooth floor.

Clausen's [4] analysis is based on the observation that the logarithmic part of the velocity profile undergoes a parallel downward shift due to surface roughness, and the amount of shift $\frac{\Delta U}{u_*}$ is a function of the parameter $u_* k/\nu$, and is directly related to the increase in surface

shear stress due to the roughness. This latter relation is found to be logarithmic, so that for a fully rough situation the velocity distribution becomes

$$\frac{U}{u_*} = 5.6 \log \frac{y}{k} + \text{const} \quad (13)$$

which is independent of the viscosity and consequently of the Reynolds number. Using Clausers analysis Hama has further shown that the local drag coefficient is independent of the Reynolds number for a constant value of

$\frac{\delta_*}{k}$ or $\frac{\theta}{k}$ instead of the ratio $\frac{x}{k}$ in the Prandtl-Schlichting resistance chart. It may be noted that since the boundary layers are usually made turbulent artificially near the leading edge, its origin does not coincide with the leading edge. Thus the parameters δ_* and θ appear to be more meaningful than the rather arbitrary distance x .

Rotta [18] has further shown that for aerodynamically smooth surfaces drag coefficient is independent of k/θ . With increasing heights of roughness the ratio k/θ gains more and more influence relative to $\frac{U_\infty \theta}{v}$, until finally for the limiting case of the fully rough surface, c_f is a function of k/θ and H only.

Flow Modification due to an abrupt roughness change: --

The analysis referred to so far considered only a homogeneous rough surface starting from the leading edge. However such situations only seldom arise in practice particularly in atmospheric flows. Any abrupt change in surface roughness modifies the flow pattern downstream,

and its study is of considerable practical interest in meteorology, air pollution, aviation and so forth. In recent years some analytical treatments using simplified models and much less experimental studies and field measurements have been made for the two-dimensional situation. We shall briefly review some of the important findings of these investigations.

One of the earliest works along these lines was due to Elliot [5]. He assumed that close to the wall the adjustments of flow takes place almost immediately, but in the outer part the effect is not felt at least in the earlier stages. Downstream of the roughness change an internal layer grows as the $4/5$ th power of the distance downwind and is independent of the windspeed. Inside this internal layer the mean velocity is assumed to have a logarithmic profile corresponding to the local wall shear stress and the roughness length, but outside of this layer the original unperturbed mean velocity profile is assumed to be retained. His theory predicts a wall shear stress which increases or decreases with distance downwind depending on whether the roughness length decreases or increases at the discontinuity. This is in qualitative agreement with observations.

Panofsky and Townsend [15] modified Elliots analysis and obtained the slope of the interface of the order of $1/10$. Townsend [25,26,27] observed that the development of the flow modification is self-preserving. Blom and

Wartena [2] recently extended and supposedly corrected some discrepancies of Townsends theory to obtain nearly same wind profiles but greatly different values of surface shear stress. They extended the theory to two or more subsequent changes in surface roughness. Taylor [23] used the mixing length concept to relate the shear stress to the velocity profiles. His results are mostly qualitative in nature.

Peterson [16] used a slightly different approach and assumed that the shear stress is proportional to the turbulent energy. The momentum, continuity and turbulent energy equations were solved numerically. The surface shear stress distribution downstream of the roughness change agrees fairly well with some field data observed by Bradley [3]. The velocity profiles were found to have an inflexion point in the transition region which is also in agreement with some field and wind tunnel data.

Only very few field observations of wind profile modification and shear stress distribution have been reported so far. Direct observations of surface shear stress for homogeneous surfaces have been made by Sheppard, Pasquill, Vehrencamp, Rider and others, some of which are briefly reported in ref. [11]. John Hopkins University Laboratory of Climatology used a duplicate of Sheppards original design with some alterations. University of California has also used an instrument for measurements with grass surfaces. These are also reported in ref. [11].

All these instruments essentially consisted of a floating plate flush with the surface and attached to a spring element.

Bradley [3] has reported some field measurements of velocity profiles and surface drag downstream of abrupt changes in surface conditions. His measurements indicate a rather rapid return of the surface shear stress to the constant downstream value. The velocity profiles agreed fairly well with those predicted by Panofsky and Townsend [15] except for an inflection point in the smooth to rough transition which is predicted by Peterson [16].

Laboratory investigation gives a better understanding of the problem since measurements can be made under controlled and stationary conditions. Some wind tunnel studies have been reported using essentially two dimensional changes in surface roughness. Jacobs [10] was the first to study this problem experimentally for pipe flow with an abrupt change in surface roughness. The shear stress was found by fitting the velocity profile into a logarithmic distribution. He found that the shear stress attains its equilibrium value almost immediately after the change of roughness. Measurements made by Logan and Jones [12] for pipe flows, Taylor [24] and Makita [14] in wind tunnels indicate that the wall shear stress overshoots the equilibrium value downstream and gradually returns back to the equilibrium value.

Antonia and Luxton [1] have analysed their results from wind tunnel measurements in a different manner. Instead of using the law of the wall they found that the velocity varied as $y^{1/2}$ using dimensional arguments. The internal boundary layer, defined as the distance from the wall to the kneepoint between the two linear parts of the U versus $y^{1/2}$ plot, is found to grow as $x^{0.5}$. Estimation of the wall shear stress is not reported.

Thus the results of the above investigations along with the field measurements made by Bradley [3] gives a definite indication that the surface shear stress at the roughness change overshoots the equilibrium value to which it returns gradually.

It is to be noted, however that all these investigations were applied to the case where fully developed flow had been established before the change in surface roughness. The purpose of these investigations was to obtain information on the flow modifications downstream of a two dimensional roughness discontinuity. The wall shear stress was estimated by fitting the mean velocity profiles into logarithmic distribution. Only the fully rough situation was studied and the effects of Reynolds number and three dimensional changes in surface roughness were not studied. Also no direct measurement of shear stress on rough surfaces has been reported so far. The present investigation is an attempt to use a shear plate to measure the surface shear stress directly when a finite size of

roughness is placed in an otherwise smooth floor of the wind tunnel. The measurements were made by keeping the rough surface at different locations in a developing boundary layer using different velocities, so as to obtain a large variation in the Reynolds number of the flow. Chapter 3 describes the experimental arrangement and methods of measurements used in the present investigation.

CHAPTER 3

EXPERIMENTAL EQUIPMENT AND PROCEDURE

Wind Tunnel: --

The experiments were conducted in the Army Meteorological Wind Tunnel at the Colorado State University Fluid Dynamics and Diffusion Laboratory. The tunnel has a 90 ft. long test section and a nominal cross-section of 6 ft. by 6 ft. Fig. 1 shows plan of this wind tunnel. The movable ceiling can be adjusted to obtain zero, negative or positive longitudinal pressure gradients. A large contraction ratio of 9:1 along with four damping screens give a free stream turbulence level of about 0.1%. The tunnel is of the recirculating type but can be used for open loop operation also. Mean velocities from 0 to 120 fps. can be attained in the test section. A detailed description of this wind tunnel facility has been given by Plate and Cermak [17].

Instrumentation:

Shear Plate: Drag measurements were made using a shear plate consisting of a floating aluminum plate of size 23.6 in. x 23.45 in. x 0.25 in. thick. Three 0.25 in. diameter hard steel balls separated this plate from the foundation plate. The two plates were connected together by means of two spring arms on each of which were installed two semiconductor strain gauges. This instrument was designed and built by J. H. Nath at the Colorado State

University. Details of the construction and working of the shear plate as well as the strain gauge force dynamometer are explained in the reports by Hsi and Nath [8,9]. A stable five-volt D.C. power supply was used to excite the strain gauges and the output was read using a D.C. Microvoltammeter after passing it through a circuit bridge arrangement. The arrangements were essentially the same as used by Hsi and Nath.

Force Dynamometer: Exploratory studies have been made using the strain gauge force dynamometer used by Hsi and Nath. They used this instrument for measuring the drag on a single model tree attached to its top. For the present study it was slightly modified by attaching a thin 3 in. x 3 in. smooth horizontal brass plate on its top. The circuit bridge used by them was also modified for better operation at low drag forces, as shown in Fig. 3. The rest of the arrangements were again essentially the same as used by Hsi and Nath.

Pitot-static Tube: --

A 1/8 in. diameter Pitot-static tube was used for all velocity measurements in the present investigation. This was connected by plastic tubing to a Transonics Equibar Type 120B electronic manometer which gave the difference in static and dynamic pressures. The output of the pressure meter was connected to the Y of an X-Y recorder. The X of the recorder received the output voltage of the potentiometer device attached to the wind

tunnel carriage on which Pitot-static tube was mounted. Thus a continuous velocity signal with distance could be recorded.

Surface Roughness: --

The rough surface in the present investigation consisted of 0.25 in. masonite board cut into 0.5 in. square elements and carefully stuck on to a vinyl cloth with 0.25 in. space between each element. There were 31 rows and columns making up a size of 23.25 in. square area to fit on top of the shear plate almost exactly. Fig. 2.a shows the arrangement of the roughness elements. For making measurements with this rough surface in position a large number of double stick tapes were placed across and along the surface of the shear plate on which the rough surface was carefully stuck in position.

Calibration: --

The shear plate and the force-dynamometer were calibrated in the manner described by Hsi and Nath [9]. Good repeatability was observed for the calibration curves which were very linear. The shear plate was calibrated before setting it up in the seven different locations along the wind tunnel floor. The differences if they existed were very insignificant. The calibration curves for the shear plate and the face dynamometer are shown in Figs. 4 and 5.

Procedure: --

One of the major objectives of the investigation involved the determination of whether the roughness used in the present study behaved like a fully rough surface under the normal testing conditions in the wind tunnel. For this purpose it was necessary to obtain a wide range of Reynolds numbers. Seven different locations along the wind tunnel floor and five different free-stream velocities for each location were used. The X-distances measured from the end of the trip device to the centre of the shear plate were $X = 3, 10, 20, 30, 45, 60$ and 85 ft. (called stations 1 through 8) and the velocities were $U_{\infty} = 10, 20, 30, 40,$ and 50 fps. The general arrangement of the setup is shown in Fig. 2.b.

At each of these locations the shear plate was aligned along the centerline of the floor at the measured distance. 0.75 in. thick particle boards 3 ft. long and 2 ft. wide and having a smooth finish were placed across the entire tunnel width both upstream and downstream of the shear plate. The upstream floor extended up to about 16 ft. from the shear plate where a gradual transition was provided by means of an 8 in. ramp. The downstream floor extended to about 6 to 9 ft. All joints were carefully taped to provide a smooth surface.

The Pitot-static tube was mounted on the wind tunnel carriage directly over the shear plate and well above the boundary layer. The shear plate (smooth) was now ready for

operation. In this position with no flow in the wind tunnel the circuit bridge was adjusted to obtain a null reading of the microvoltmeter. The air flow was then adjusted to 10 fps. ambient velocity and the output was read. The flow was shut off and zero reading was checked. An average value of velocity and drag was obtained from two or three repetitions. This procedure was used for the five velocities. The roughness was then placed over the shear plate and similar drag measurements were made.

With smooth as well as rough surfaces velocity profiles were obtained at the centre of the plate for the five velocities. At one representative station 4 ($X = 30$ ft.) and $U_{\infty} = 30$ fps. velocity profiles were taken along the centerline of the shear plate for the smooth and rough surfaces at intervals of 3 ins., and downstream of the shear plate at 6 ins. intervals at four locations.

At station 7 ($X = 85$ ft.) some exploratory measurements were made using the 3 in. square force dynamometer plate in order to find the variation of local shear stress along the rough surface. The force dynamometer was fixed under the floor of the wind tunnel, the 3 in. square plate reaching up to the surface through a properly aligned square hole. The gap around the plate was about 1 mm.

Drag measurements were made with the smooth plate for $U = 30$ fps. and 40 fps. The two feet square roughness was cut into proper sizes and arranged around and on the plate

such that the plate was at the centre of the leading edge of the rough area. Drag was measured in this position for two velocities, 30 and 40 fps. Keeping the plate in the same position, the roughness around it was successively moved 3 in. upstream, each time measuring the drag force. Since the flow in this region was very nearly fully developed, this procedure could be expected to indicate the variation of local wall shear stress along the centre of the rough area.

The results obtained from these experiments are discussed in Chapter 4.

CHAPTER 4

RESULTS AND DISCUSSIONS

The method of analysis of the data and discussions on the results are given in this chapter. Most of the computations for reducing the data obtained from the experiments were done using the CDC 6400 computer facility available at the Colorado State University.

Local Drag Coefficient: --

The local drag coefficient $c_f = \frac{\tau_o}{\frac{1}{2}\rho U_\infty^2}$ was calculated from the output of the shear plate strain gauge device using its calibration curve. The surface shear stress τ_o was actually taken as the average for the entire surface area of the shear plate without considering the variations along and across the smooth or rough surface. The justification for this stems from the reasonable assumption that these variations are rather small. The effects of this variation on the average value for different flow conditions are, however, proposed to be examined at a later stage.

In order to find out whether the roughness used in this study behaves like an aerodynamically rough surface, it is necessary to obtain the variation of the local drag coefficient with the Reynolds number of the flow. For this purpose a Reynolds number R_{x_e} was defined as

$\frac{U_{\infty} x_e}{\nu}$ based on the effective distance x_e from a virtual origin of the turbulent boundary layer. Because of the 6 ft long rough surface provided at the entrance to the wind tunnel for artificially thickening the boundary layer, true flat plate conditions are not obtained in the wind tunnel. This makes it necessary to obtain the virtual origin. There is no method which gives the exact location of this virtual origin. The method adopted in the present study was based on the variation of the momentum thickness with x for a flat plate boundary layer. Equation (4) obtained by Schlichting [19] using 1/7-power law velocity distribution was used. The smooth surface velocity profiles exhibited such distribution in the present study. A typical profile is shown in Fig. 12.a.

The velocity profiles were integrated numerically using Simpsons rule to obtain the momentum thickness θ at each station. The effective distance x_e were then calculated using equation (4). The Reynolds numbers were thus obtained for the smooth and rough cases using the same value of x_e . Fig. 6 shows a plot of the local drag coefficient variation with R_{x_e} for the smooth and rough surfaces. It may be observed from this plot that for the smooth surface the drag coefficient follows the curves of Schlichting and Smith and Walker fairly closely. The scatter may perhaps be due to errors in the evaluation of

c_f . However, the results obtained at the first station ($x = 3$ ft) fall much below the rest of the values, suggesting dependence on another parameter. On closer examination this appears to be the shape parameter H . The values of H at $x = 3$ ft are much higher (about 1.48) than at other stations (average about 1.27). There is an apparent decrease in the drag coefficient with increase in H . This dependence is in reasonable agreement with the results of some of the earlier investigations. (see Rotta [18]).

For the rough surface the scatter is again marked, although an average constant value of about 7×10^{-3} may be observed, and this fact may be taken to mean that the surface is fully rough. However, as for the smooth surface the functional dependence on the shape parameter H is again valid for the rough surface too. Yet another parameter, the ratio k/θ also influences the drag coefficient. It is observed that for a given value of the shape parameter H , the drag coefficient tend to increase with an increase in the ratio k/θ .

The situation becomes easier for comparison with Rotta's [18] formulation when the c_f values are plotted against the momentum thickness Reynolds number $R_\theta = \frac{U_\infty \theta}{\nu}$. Such a plot is shown in Fig. 7. The drag coefficient for the rough surface is thus a function of at least three independent parameters, $\frac{U_\infty \theta}{\nu}$, which shows no influence for

the fully rough situation, H , and the ratio k/θ the influence of which increases for larger ratios. For the present case, at least two more factors may find their influence in some manner. On the one hand, the effect of the abrupt change from smooth to rough surface and on the other, the effect of three-dimensional nature of the rough area need to be investigated. Yet another factor which needs to be studied is the error involved because of the averaging of the shear stress over the entire rough area instead of considering the true local shear stresses.

Local Surface Shear Measurements Along Roughness: --

The results of the exploratory drag measurements using the force dynamometer are shown in Fig. 8. The local drag coefficient measured by this instrument for the smooth case is about 15% larger than the value obtained by using shear plate; and for the rough surface, the average value is over 25% smaller than the shear plate value. The reason for these large differences may be that even small differences in the levels of the plate and the tunnel floor may increase or decrease the measured drag. However, for the two mean velocities tested the definite trend in the variation of the local drag coefficient downstream of the roughness change can be noticed. Just at the roughness discontinuity the drag coefficient overshoots to a much larger value than the average or equilibrium

value. There is then a rapid drop in the drag coefficient. Most of the change seems to occur in the first three or four inches. This shows that the averaged value obtained by using the shear plate is fairly representative of the local drag coefficient except in the vicinity of the roughness change. The force dynamometer as well as the measuring techniques need to be improved for making some reliable measurements along these lines.

Velocity Profiles: --

As mentioned in Chapter 2 most of the reported shear stress measurements on rough surfaces were done by fitting the lower part of the velocity profile into a logarithmic distribution. This possibility was checked for the present case for comparison with the direct measurements. Fig. 9 shows such a plot at the center of smooth and the rough surfaces at Station 5 ($x = 44$ ft) for an ambient velocity $U_{\infty} = 30$ fps. Similar plots were made at other stations and for other velocities. They show that the logarithmic distribution no longer exists over the rough surface. More detailed plots are shown in Figs. 10. a & b, which show the semilogarithmic plot of the velocity profiles taken at different distances along the centerline of the rough surface and downstream at station 4 ($x = 30$ ft) for $U_{\infty} = 30$ fps. and for the same situation over the smooth surface. While the smooth surface profile clearly shows a logarithmic

$$\text{region of the form, } \frac{U}{u_*} = 5.57 \log \frac{yu_*}{v} + 4.83 \quad (14)$$

for the rough surface a straight line portion in the wall region is hardly discernible. Even along the smooth floor downstream of the rough surface, (Fig. 10.b) the velocity profiles continue to have the same shape even at about 20 in. from the last row of roughness elements. One possible explanation for the absence of a log profile over the rough area in the present study is that all these profiles were taken between two roughness elements which may not be truly representative of the general velocity distribution over the entire rough surface. An average mean velocity taken across two roughness elements at different heights above the surface may give a more significant velocity distribution.

Fig. 11 is a combined plot of all such profiles over the rough surface and downstream of it. The dimensionless velocity U/U_∞ has been used for comparison. It may be noticed that above about 1.5 in. all the profiles almost merge on to the smooth surface profile. The deviations of the profiles below this height are somewhat similar to the form predicted by the theories of Townsend [26,27], Peterson [16] and others and to the profiles measured by Bradley [3]. However the straight line portion appear to be below 0.2 in. where accurate measurements of velocity could not be made.

Figure 12.a is a representative power-law profile of the form

$$\frac{U}{U_{\infty}} = (y/\delta)^{1/n} \quad (15)$$

It may easily be observed that such a relation appears to be valid for the entire boundary layer thickness. For the present study the value of n ranged from about 6.8 to 7.6. Similar profiles are shown for the rough surface in Fig. 12 (b through f). In the lower part of these profiles there is a definite change in the slope perhaps up to the height influenced by the roughness. The slope is much flatter here than above it. However, a strict power law does not seem to exist near the wall. Another way of plotting these profiles is to use $y^{1/2}$ instead of y , the height being measured above the top of the roughness elements. This gives two linear relationships, one near the wall and one away from it. Fig. 13 shows such a plot. This is in fair agreement with the observations of Antonia and Luxton [1]. The point where the slope changes has been taken to be the edge of the internal boundary layer by these authors. In the present study no further observations on these lines have been made so far; this possibly includes the behavior of the numerical coefficients and constants of such a plot under different flow conditions.

General Discussion: --

A simple plot of the local drag coefficient variation with the Reynolds number (R_{x_e} or R_{θ}) for a rough surface thus does not directly show whether the surface is fully

rough or not, since the shape parameter H and the ratio k/θ also influences the drag coefficient considerably. However, for most of the wind tunnel conditions, the variation of H is very small except perhaps for very low velocities. Thus for practical purposes one may use a c_f vs R_θ plot to determine whether the surface is fully rough or not. One may thus also use the $\frac{u_*^* k}{v}$ criterion. Figure 14 shows a plot of all values of $\frac{u_*^* k}{v}$ in this study against the Reynolds number R_{x_e} . The variation is similar for all the stations, and apparently the value of $\frac{u_*^* k}{v}$ does not change much with x for a given velocity. The lowest values are between 60 and 70 for $U_\infty = 10$ fps. This value is consistent with the minimum value for which a surface is fully rough. Thus these results show that as long as the velocity is above 10 fps. the rough boundary used in the present study behaves like a fully rough surface.

The measured and calculated quantities and parameters are tabulated in Tables 1 through 7.

CHAPTER 5

CONCLUSIONS

The present experimental study has led to the following conclusions:

1. The particular roughness size and arrangement studied behaves like a fully rough boundary for mean velocities over 10 fps.
2. There is some evidence, by means of the force dynamometer measurements, to show that most of the variation in surface shear stress after the change of roughness occurs within the initial 3 in. or 4 in. Therefore, the shear plate measurements are very nearly the same as the equilibrium shear stress over the surface. Also, the shear plate measurements for the smooth surface are in reasonably good agreement with the predicted values of earlier investigations. Thus the shear plate can be successfully used for measuring drag on smooth as well as rough boundaries.
3. The Reynolds number based on the momentum thickness θ (i.e., $R_\theta = \frac{U_\infty \theta}{\nu}$) appears to be a better parameter than the one based on the x-distance ($R_x = \frac{U_\infty x}{\nu}$).

Also there is no exact way of calculating the virtual origin of the turbulent boundary layer or the effective distance X_e , which also justifies

the use of R_θ . However, the influence of the shape parameter H and the ratio k/θ also need to be considered.

4. Velocity profiles over the rough surface do not show logarithmic distribution in the present case. Therefore the wall shear stress cannot be obtained from these profiles. However, if the mean velocities are averaged in the lateral direction across one or two roughness elements at different heights a more representative velocity distribution might result. In the present study power-law velocity profiles showed definite characteristics, with two distinct parts. The point where the slope changes suddenly may be used effectively to define the edge of the internal boundary layer.

REFERENCES

1. Antonia, R. A., and R. E. Luxton, (1968), "The Response of a Turbulent Boundary Layer to a Step Change in Surface Roughness," Dept. of Mech. Eng., Univ. of Sydney.
2. Blom, J., and L. Wartena, (1969), "The Influence of Changes in Surface Roughness on the Development of the Atmosphere," Journal of the Atmospheric Sciences, 26, 1969.
3. Bradley, E. F., (1968), "A Micrometeorological Study of Velocity Profiles and Surface Drag in the Region Modified by a Change in Surface Roughness," Quart. J. Roy. Met. Soc., 94.
4. Clauser, F. H., (1956), "The Turbulent Boundary Layer," Advances Appl. Mech. 4, New York, N. Y.
5. Elliott, W. P., (1958), "The Growth of the Atmospheric Internal Boundary Layer," Trans. Amer. Geophys. Union, 39, No. 6.
6. Hama, F. R., (1954), "Boundary Layer Characteristics for Smooth and Rough Surfaces," Trans. Soc. Naval Arch. and Marine Engrs., 62.
7. Hinze, J. O., (1959), "Turbulence," McGraw Hill, New York.
8. Hsi, G., and J. H. Nath, (1968), "A Laboratory Study on the Drag Force Distribution Within Model Forest Canopies in Turbulent Shear Flow," Fluid Dynamics and Diffusion Laboratory, Colorado State University, Report No. CER67-68GH-JHN50.
9. Hsi, G. and J. H. Nath, (1968), "Wind Drag Within a Simulated Forest Canopy Field," Fluid Dynamics and Diffusion Laboratory, Colorado State University, Report No. CER68-69GH-JHN6.
10. Jacobs, W., (1940), "Variation in Velocity Profile With Change in Surface Roughness of Boundary," NACA-TM 951.
11. Lettau, H. H., and B. Davidson, (1957), "Exploring the Atmosphere's First Mile," Vol. 1, Pergamon Press, N. Y.
12. Logan, E. and J. B. Jones, (1963), "Flow in a Pipe Following an Abrupt Increase in Surface Roughness," Trans. ASME, 85, D 35.

13. Ludwig, H., and W. Tillman, (1950), "Investigation of Wall Shearing Stress in Turbulent Boundary Layer," NACA-TM 1285.
14. Makita, H., (1968), "Response of a Turbulent Boundary Layer to a Sudden Change in Surface Roughness," M. Eng. Thesis, Univ. of Tokyo.
15. Panofsky, H. A., and A. A. Townsend, (1964), "Change of Terrain Roughness and the Wind Profile," Quart. J. Roy. Met. Soc. 90.
16. Peterson, E. W., (1969), "Modification of Mean Flow and Turbulent Energy by a Change in Surface Roughness under Conditions of Neutral Stability," Quart. J. Roy. Met. Soc. 95.
17. Plate, E. J., and J. E. Cermak, (1963), "Micrometeorological Wind Tunnel Facility," Final Report, Fluid Dynamics and Diffusion Laboratory, Colorado State University, Report No. CER63EJP-JEC9.
18. Rotta, J. E., (1962), "Turbulent Boundary Layers in Incompressible Flows," Progress in Aeronautical Sciences, Vol. 2, MacMillan Co., New York.
19. Schlichting, H., (1968), "Boundary Layer Theory," McGraw Hill, New York.
20. Schubauer, G. B., and Klebanoff, P. S., (1951), "Investigation of Separation of the Turbulent Boundary Layer," NACA-Rep. 1030.
21. Schultz-Grunow, F., (1941), "New Frictional Resistance Law for Smooth Plates," NACA-TM 986.
22. Smith, D. W., and J. H. Walker, (1958), "Skin Friction Measurements in Incompressible Flow," NACA T.N. 4231.
23. Taylor, P. A., "On Wind and Shear Stress Profiles Over a Change in Surface Roughness," Quart. J. of Roy. Met. Soc., 95, 1969.
24. Taylor, R. J., "Small Scale Advection and the Neutral Wind Profile," J. Fluid Mech. 13, 1962.
- 25,26 Townsend, A. A., (1965), "Self Preserving Flow Inside a Turbulent Boundary Layer," and "Response of a Turbulent Boundary Layer to Abrupt Changes in Surface Roughness," J. Fluid Mech. 22, Pt. 4.
27. Townsend, A. A., (1966), "The Flow in a Turbulent Boundary Layer After a Change in Surface Roughness," J. Fluid Mech. 26, Pt. 2.

TABLE: 1
x = 3 ft.

U fps.	δ in.*	θ in.	H	x_e ft.	$R_{x_e} \times 10^{-7}$	$R_\theta \times 10^{-4}$	$c_f \times 10^{-3}$ smooth	$c_f \times 10^{-3}$ rough	$\frac{U_* k}{v}$	$\frac{k}{\theta}$
10.25	0.833	0.550	1.513	20.4	0.104	0.235	2.77	6.73	61.9	
19.8	0.801	0.542	1.480	23.6	0.232	0.45	2.35	6.73	120	
30.35	0.810	0.545	1.486	26.4	0.40	0.69	2.13	6.42	179	
40.6	0.817	0.553	1.476	28.9	0.586	0.935	1.94	6.63	243	
49.85	0.839	0.570	1.472	31.6	0.788	1.12	1.85	6.56	297	

TABLE: 2
x = 10 ft

U fps.	δ in.*	θ in.	H	x_e ft.	$R_{x_e} \times 10^{-7}$	$R_\theta \times 10^{-4}$	$c_f \times 10^{-3}$ smooth	$c_f \times 10^{-3}$ rough	$\frac{U_* k}{v}$	$\frac{k}{\theta}$
10.2	0.886	0.665	1.332	25.8	0.131	0.283	3.21	7.8	66	
20.25	0.867	0.667	1.299	30.7	0.311	0.563	2.92	7.95	129	
30.18	0.86	0.672	1.277	34.25	0.517	0.845	2.68	7.37	189	
40.5	0.875	0.686	1.276	37.8	0.765	1.16	2.6	7.11	248	
50.3	0.84	0.663	1.265	38.25	0.961	1.39	2.58	7.23	309	

TABLE: 3
x = 20 ft.

U fps.	δ_* in.	θ in.	H	x_e ft.	$R_{x_e} \times 10^{-7}$	$R_\theta \times 10^{-4}$	$c_f \times 10^{-3}$ smooth	$c_f \times 10^{-3}$ rough	$\frac{U_* k}{v}$	$\frac{k}{\theta}$
10.03	1.231	0.978	1.26	41.6	0.208	0.41	3.37	7.88	65.6	
19.71	1.389	1.101	1.262	57.1	0.564	0.904	3.02	8.09	131.0	
29.86	1.331	1.074	1.24	61.4	0.919	1.34	2.83	7.91	194.3	
39.63	1.289	1.036	1.244	63.0	1.25	1.71	2.63	7.64	256	
49.42	1.299	1.043	1.245	67.1	1.66	2.15	2.56	7.9	322	
60.0	1.241	1.007	1.232	67.4	2.03	2.51	2.49	8.11	396	

TABLE: 4
x = 40 ft.

U fps.	δ_* in.	θ in.	H	x_e ft.	$R_{x_e} \times 10^{-7}$	$R_\theta \times 10^{-4}$	$c_f \times 10^{-3}$ smooth	$c_f \times 10^{-3}$ rough	$\frac{U_* k}{v}$	$\frac{k}{\theta}$
10.4	1.386	1.063	1.304	46.5	0.242	0.46	3.73	7.39	65.2	
20.1	1.652	1.293	1.278	70.1	0.705	1.08	3.0	7.05	123.0	
30.05	1.509	1.189	1.269	69.8	1.05	1.49	2.69	6.93	182.5	
40.0	1.548	1.236	1.253	78.7	1.57	2.05	2.6	6.83	241.0	
50.2	1.541	1.241	1.242	83.7	2.10	2.6	2.6	6.86	303.5	

TABLE: 5
x = 45 ft.

U fps.	δ_* in.	θ in.	H	x_e ft.	$R_{x_e} \times 10^{-7}$	$R_\theta \times 10^{-4}$	$c_f \times 10^{-3}$ smooth	$c_f \times 10^{-3}$ rough	$\frac{U_* k}{v}$	$\frac{k}{\theta}$
9.85	1.866	1.447	1.290	67.5	0.332	0.586	3.6	7.38	62.6	
19.72	2.136	1.660	1.287	95.4	0.943	1.363	2.88	7.25	124	
29.75	1.985	1.555	1.277	97.4	1.53	1.926	2.62	7.09	183.6	
39.89	1.893	1.502	1.260	100.4	2.01	2.5	2.5	7.09	247	
49.57	1.921	1.530	1.255	108.5	2.69	3.16	2.43	7.37	313	
59.51	1.831	1.459	1.255	107.0	3.19	3.616	2.36	7.63	382.6	
79.46	1.846	1.473	1.253	116.4	4.64	4.88	--	8.48	535	

TABLE: 6
x = 60 ft.

U fps.	δ_* in.	θ in.	H	x_e ft.	$R_{x_e} \times 10^{-7}$	$R_\theta \times 10^{-4}$	$c_f \times 10^{-3}$ smooth	$c_f \times 10^{-3}$ rough	$\frac{U_* k}{v}$	$\frac{k}{\theta}$
9.66	2.527	1.846	1.369	91.25	0.444	0.743	3.08	8.46	68.1	
19.61	2.495	1.830	1.364	107.75	1.064	1.495	2.91	7.53	127.2	
29.58	2.349	1.816	1.293	118.3	1.762	2.235	2.67	7.25	188.5	
39.73	2.404	1.854	1.297	130.7	2.615	3.07	2.42	7.28	252.0	
49.65	2.221	1.724	1.288	126.0	3.133	3.567	2.35	7.36	314.7	
59.49	2.174	1.712	1.270	130.7	3.893	4.24	2.09	7.66	385.0	

TABLE: 7
x = 85 ft.

U fps.	δ_* in.	θ in.	H	x_e ft.	$R_{x_e} \times 10^{-7}$	$R_\theta \times 10^{-4}$	$c_f \times 10^{-3}$ smooth	$c_f \times 10^{-3}$ rough	$\frac{U_* k}{v}$	$\frac{k}{\theta}$
10.5	2.766	2.150	1.287	112.5	0.591	0.94	2.28	6.62	63	
19.5	3.046	2.374	1.283	148.7	1.45	1.93	1.98	6.52	114	
29.53	3.021	2.359	1.281	163.6	2.416	2.9	2.28	6.23	170.5	
39.62	2.945	2.321	1.269	172.6	3.42	3.833	2.13	6.26	229.5	
49.85	2.862	2.265	1.263	177.3	4.42	4.71	2.0	6.39	286	